# Visible-blind and solar-blind ultraviolet photodiodes based on $(In_xGa_{1-x})_2O_3$

Zhipeng Zhang, Holger von Wenckstern, Jörg Lenzner, Michael Lorenz, and Marius Grundmann

---

**Articles you may be interested in**

Wavelength-selective ultraviolet (Mg,Zn)O photodiodes: Tuning of parallel composition gradients with oxygen pressure
Applied Physics Letters **108**, 243503 (2016); 10.1063/1.4954375

Gallium oxide ($Ga_2O_3$) metal-semiconductor field-effect transistors on single-crystal $\beta$-$Ga_2O_3$ (010) substrates
Applied Physics Letters **100**, 013504 (2012); 10.1063/1.3674287

Deep-ultraviolet transparent conductive $\beta - Ga_2O_3$ thin films
Applied Physics Letters **77**, 4166 (2000); 10.1063/1.1330559

Oxygen vacancies and donor impurities in $\beta - Ga_2O_3$
Applied Physics Letters **97**, 142106 (2010); 10.1063/1.3499306

Oxygen vacancy tuned Ohmic-Schottky conversion for enhanced performance in $\beta$-$Ga_2O_3$ solar-blind ultraviolet photodetectors
Applied Physics Letters **105**, 023507 (2014); 10.1063/1.4890524

Crystal Structure of $\beta$-$Ga_2O_3$
The Journal of Chemical Physics **33**, 676 (1960); 10.1063/1.1731237

---

# Visible-blind and solar-blind ultraviolet photodiodes based on $(In_xGa_{1−x})_2O_3$

Zhipeng Zhang, Holger von Wenckstern, Jörg Lenzner, Michael Lorenz, and Marius Grundmann

*Institut für Experimentelle Physik II, Fakultät für Physik und Geowissenschaften, Universität Leipzig, Linnéstraße 5, 04103 Leipzig, Germany*

UV and deep-UV selective photodiodes from visible-blind to solar-blind were realized based on a Si-doped $(In_xGa_{1−x})_2O_3$ thin film with a monotonic lateral variation of $0.0035 < x < 0.83$. Such layer was deposited by employing a continuous composition spread approach relying on the ablation of a single segmented target in pulsed-laser deposition. The photo response signal is provided from a metal-semiconductor-metal structure upon backside illumination. The absorption onset was tuned from 4.83 to 3.22 eV for increasing $x$. Higher responsivities were observed for photodiodes fabricated from indium-rich part of the sample, for which an internal gain mechanism could be identified. © 2016 AIP Publishing LLC. [http://dx.doi.org/10.1063/1.4944860]

Ultraviolet photodiodes (UV PDs) based on wide bandgap semiconductors find applications for surveillance purpose, remote sensing, medical monitoring, and biological agent sensors.[1] Good candidates are, e.g., (Al,Ga)N,[1–3] (Mg,Zn)O,[4–7] (Ni,Mg)O,[8] (Zr,Ti)O$_2$,[9] and diamond.[10,11] Group-III sesquioxide compounds including In$_2$O$_3$[12–17] and $β$-Ga$_2$O$_3$[18–23] have interesting physical properties such as large bandgap $E_g$ from 2.9 eV for In$_2$O$_3$[14] to 4.9 eV for $β$-Ga$_2$O$_3$.[18] Alloying Ga$_2$O$_3$ with In$_2$O$_3$ offers an opportunity to tailor $E_g$[24] rendering the ternary $(In_xGa_{1−x})_2O_3$[25–34] suited for visible-blind ($λ < 400$ nm) and solar-blind ($λ < 280$ nm) UV PDs.

The cutoff energy $E_{cutoff}$ of PDs corresponds to the absorption edge of $(In_xGa_{1−x})_2O_3$ that is defined here as the photon energy at $\sqrt{1/2}\,\mathcal{R}_{max.}$, for which $\mathcal{R}_{max.}$ indicates the maximum responsivity. Only few papers reporting on UV PDs based on $(In_xGa_{1−x})_2O_3$ are available in the literature.[27,34] Note that, all PDs are fabricated on $(In_xGa_{1−x})_2O_3$ samples with low $x$, since the fabrication of the rectifying barriers on In-rich samples is more difficult due to the existence of surface electron accumulation layer (SEAL)[13,14] originating from surface oxygen vacancies. Recently, the rectification of Schottky contacts (SCs) on cubic bixbyite In$_2$O$_3$ thin films has been realized by using a reactive sputtering process[17] that is adequate for removing the SEAL.[15] In this letter, we demonstrate SCs on an $(In_xGa_{1−x})_2O_3$ thin film for $0.0035 < x < 0.83$ allowing fabrication of metal-semiconductor-metal (MSM) PDs with absorption edge ranging from 4.83 to 3.22 eV, for which the sample was grown on by means of a large-area offset pulsed laser deposition (PLD) employing a continuous composition spread (CCS) approach.[35] Very recently, we reported PDs based on an unintentionally doped CCS $(In_xGa_{1−x})_2O_3$ thin film,[31] for which the high series resistance $R_S$ of the thin film limited the performance of PDs fabricated thereon. Therefore, a Si-doped sample has been used here since its electrical conductivity is significantly increased thereby.[19,21]

Fig. 1(a) shows the schematic layout of a MSM-PD based on a CCS $(In_xGa_{1−x})_2O_3$ thin film grown on a 2 in. in diameter one-sided polished $c$-plane sapphire wafer. To avoid unnecessary reflection and absorption by the metal electrodes, the detector is illuminated from the substrate side thus shadowing by the metal electrodes is irrelevant. Fig. 1(b) shows a deposited sample, in which the bottom left corner exhibits yellowish color indicating the In-rich part and $x$ decreases along the black dashed arrow (cf. Fig. 2(a)). The CCS approach relies on the ablation of a single segmented target consisting of two semicircular Ga$_2$O$_3$ and In$_2$O$_3$ targets. The targets are prepared by ball milling, cold pressing, and sintering for 72 h at 1350 °C and 12 h at 1600 °C, respectively. In each case, 0.1 wt. % SiO$_2$ has been admixed to each of binary targets, for which the corresponding cation share are 0.26 at. % Si in the Ga$_2$O$_3$ and 0.38 at. % Si in the In$_2$O$_3$, respectively.[32] The source material for all targets is polycrystalline powders in 5N purity. The growth temperature $T_{growth}$ and the oxygen pressure $p$ are 650 °C and 0.3 $μ$bar, respectively, which were optimized for the growth of Si-doped $β$-Ga$_2$O$_3$ PLD thin films considering their structural and electrical properties.[21]

The spatial dependence of the chemical composition of CCS $(In_xGa_{1−x})_2O_3$ thin film was investigated by energy dispersive X-ray (EDX) spectroscopy. The EDX false color representations in linear scales shown in Figs. 2(a) and 2(b) depict the spatial dependence of In- and Si-content of the sample, respectively, resulting from an interpolation from single measured point between neighboring positions visualized by black dots. A monotonic change of $x$ is observed along the In-gradient in Fig. 2(a), whereas it is essentially constant along lines lying in the perpendicular direction.
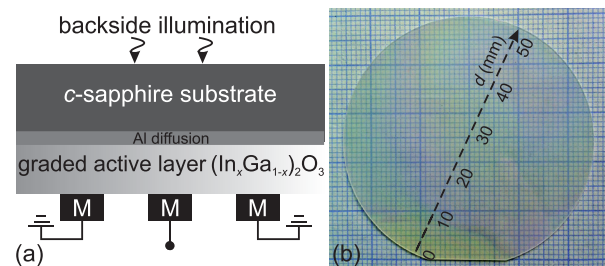


FIG. 1. (a) Schematic layout of a MSM-PD and (b) a deposited sample on a 2 in. in diameter wafer.
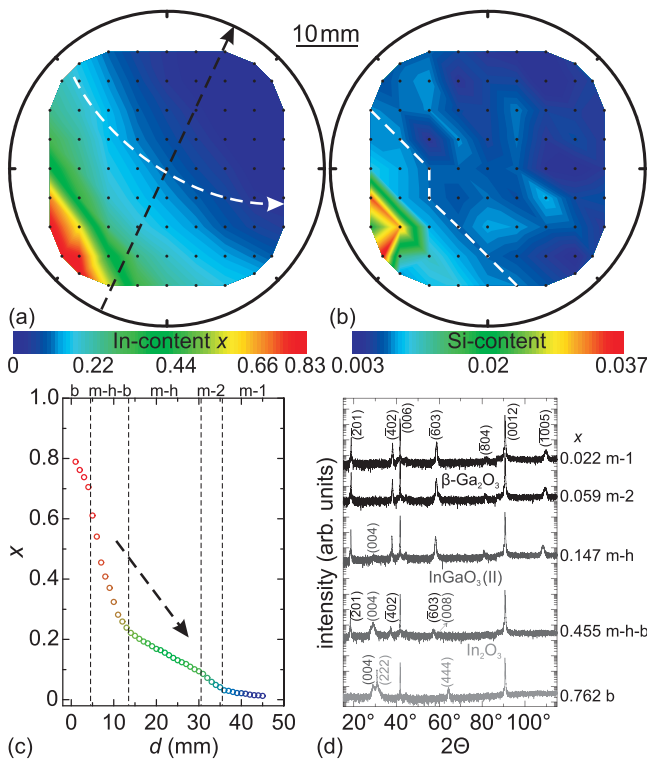
FIG. 2. EDX false color representations in linear scale of (a) In- and (b) Si-content showing the wafer, respectively; (c) EDX-line scan along the In-gradient, the black dashed lines separate different crystallographic phases; (d) single XRD patterns selected from each phase.

Similarly, two main regions of Si-content along the gradient can be distinguished from top right to bottom left part dividing by a white dashed line in Fig. 2(b). For more details about the interplay between In- and Si-incorporation, please refer to Ref. 32. Further, Fig. 2(c) depicts an EDX-line scan in dependence on spatial position $d$ along the black dashed arrow as labeled in Fig. 1(b). The nonlinear behavior is not due to the CCS approach chosen[35] that could be connected to used $c$-plane sapphire substrate[28] and explained by the formation of a few monolayers of $\alpha$-Ga$_2$O$_3$ at the interface between the sample and the substrate.[36]

The spatial particle distribution using the CCS approach was simulated by von Wenckstern *et al.* in Ref. 35. It is shown that the content within the film is typically in between the composition in of the target segments, but not reaching the limiting compositions. The maximum $x$ was obtained of about 0.83 while the minimum was measured of 0.0035 being close to zero. On one hand, the kinetic energy of the ablated particles determines the plasma expansion during the deposition; the lighter Ga-atoms are more effectively scattered on the oxygen molecules of the background gas. On the other hand, the thermodynamic effects during the deposition play a major role;[37] in this case, both binary Ga$_2$O$_3$ and In$_2$O$_3$ segmented targets have different deposition rates in dependence on $T_{\text{growth}}$.

The crystallographic properties of the sample are investigated by spatially resolved X-ray diffraction (XRD). In this letter, only exemplary single 2$\Theta$-$\omega$ scans for selected positions from each region of $d = 40, 33, 23, 7$, and 2 mm with the corresponding $x$ are shown in Fig. 2(d) from black to gray color, respectively. For $d > 36$ mm (labeled as m-1),

only peaks related to monoclinic $\beta$-Ga$_2$O$_3$ are visible. For $31 < d < 36$ mm (labeled as m-2), the thin film crystallizes as monoclinic phase without any other phases. For $14 < d < 31$ mm (labeled as m-h), the thin film crystallizes predominantly as monoclinic phase; however, starting with the appearance of hexagonal high-pressure InGaO$_3$ (II) phase.[25] For $5 < d < 14$ mm (labeled as m-h-b), besides the two other structures the cubic bixbyite In$_2$O$_3$ phase is observed indicating that three phases are present. For $d < 5$ mm (labeled as b), the sample is predominantly within the cubic bixbyite structure without the presence of monoclinic phase. Besides, the (004) reflection of hexagonal structure becomes weaker but can be still identified. Compared to the unintentionally doped sample,[31] the presence of Si can influence In-incorporation, lattice parameters, and the formation of side phases. Since Si with its fourfold coordination number occupied preferentially the tetrahedral Ga sites in (In$_x$Ga$_{1-x}$)$_2$O$_3$ alloy, the formation of hexagonal InGaO$_3$ (II) phase occurs for lower $x$ and the cubic bixbyite phases occur only for higher $x$, respectively.[32]

For fabrication of PDs, the whole wafer was divided into 50 pieces, for which each piece with a dimension of about $7 \times 5$ mm$^2$ was fully processed with the MSM-structure. The MSM-electrodes employing two SCs have been prepared by using a photolithography and reactive DC-sputtering of platinum.[7,38] Besides, for investigation of the electrical properties of the corresponding MSM-electrodes, circular SCs were fabricated by using identical parameters as the MSM-electrodes based on another sample deposited under same conditions.[32] The carrier concentration of the sample was determined in the range of $10^{17}$–$10^{18}$ cm$^{-3}$ by means of Hall-measurements using Van der Pauw method. For more details about SCs, please refer to Refs. 17, 20, 31, and 32.

Fig. 3(a) shows the spectrally resolved $\mathcal{R}$ (A/W) at an external voltage of $V_{\text{ext}} = -4.0$ V of 10 MSM-PDs for positions selected along the black dashed arrow in the direction of In-gradient (marked by black ring in Fig. 4(a)) upon backside illumination. Low photo responses are measured for $\hbar\omega < E_g$ due to the Urbach tail caused by alloy and structural disorder.[39] The maximum signal-to-noise ratio (SNR) of $\mathcal{R}$ increases up to three orders for PDs from Ga-rich region of about $x < 0.3$, which decreases to one order for In-rich part due to their decreasing Schottky barrier height $\Phi_{\text{Bn,eff}}$ and rectification ratio.[32] The graded active layer would result in a spatial dependence of the absorption edge referred to low cutoff energy $E_{\text{cutoff}}^{\text{low}}$ for $\hbar\omega < E_{\text{max}}$.[6] A blue-shift for $E_{\text{cutoff}}^{\text{low}}$ is as expected achieved for decreasing $x$ and depicted in Fig. 3(b), which depends linearly on $x$ as $E_{\text{cutoff}}^{\text{low}}(x)\,\text{eV} = (4.86 \pm 0.03)\,\text{eV} - (2.03 \pm 0.08)\,\text{eV} \cdot x$. Solid diamonds in Fig. 3(b) show the dependence of optical $E_g$ on $x$ that was determined from the absorption calculated itself from the optical transmission only. Obviously, a clear correlation between $E_{\text{cutoff}}^{\text{low}}$ and $E_g$ is observed, indicating the onset of absorption edge of sample can be tuned from UVC ($100 \leq \lambda < 280$ nm) via UVB ($280 \leq \lambda < 315$ nm) to UVA ($315 \leq \lambda < 400$ nm) for increasing $x$. Please note that the measuring spots for the EDX-measurements as shown in Fig. 2 do not exactly coincide with positions of the selected MSM-PDs.

Furthermore, $\mathcal{R}$ should extend to deep UV range by keeping a constant value for further increasing $\hbar\omega$.
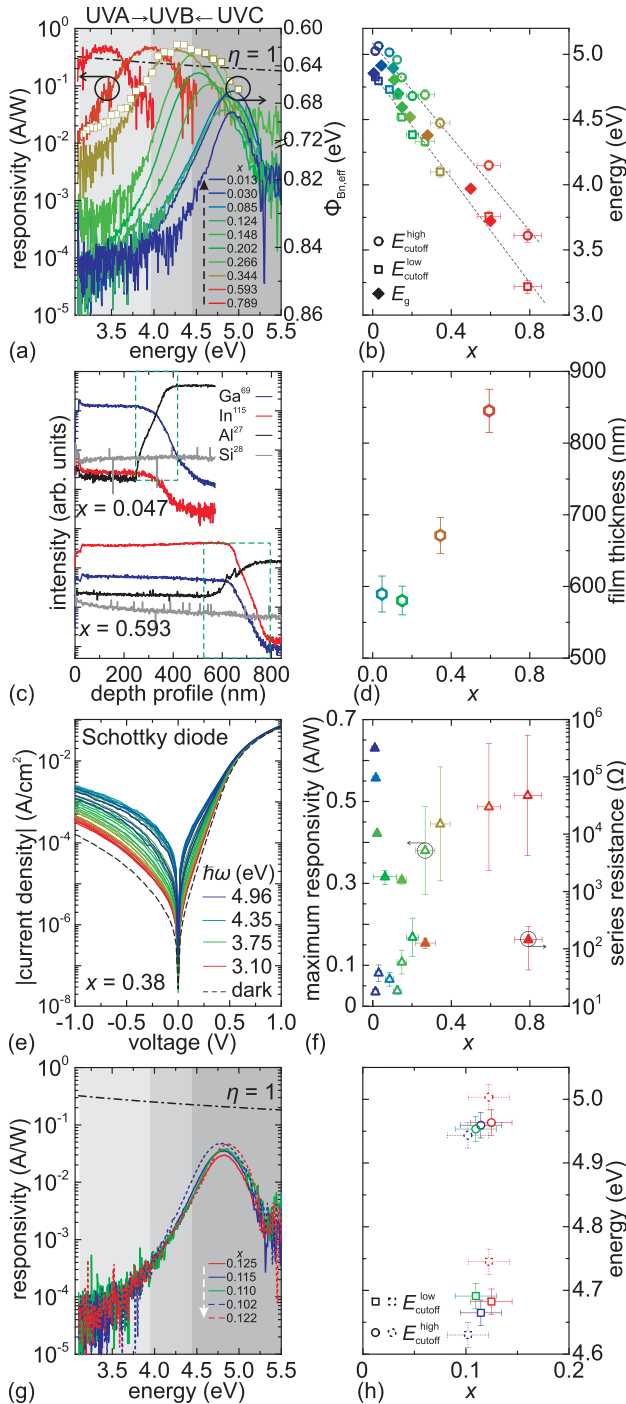
(a)                                                          (b)



FIG. 4. Contour plots of (a) $E_{cutoff}^{low}$ and (b) $E_{bandwidth}$.



FIG. 3. $\mathcal{R}$ versus $\hbar\omega$ of (a) 10 MSM-PDs along the In-gradient and (g) 5 MSM-PDs in the perpendicular direction; (b) and (h) $E_{cutoff}^{low \, (high)}$-dependence on $x$ determined from figures (a) and (g), respectively; solid diamonds in figure (b) show the $E_g$-dependence on $x$ determined by optical transmission; (c) SNMS-depth profile and (d) film thickness; (e) spectrally resolved $JV$-measurements of a SC, the analyzed $\Phi_{Bn,eff}$ are shown as squares in figure (a); (f) $\mathcal{R}_{max.}$ (open) and $R_S$ (solid) versus $x$.

Surprisingly, the $\mathcal{R}$ fell off with increasing $\hbar\omega$ such that for each device exists an upper energy limit. It results the high cutoff energies $E_{cutoff}^{high}$ for $\hbar\omega > E_{max.}$ that decreases also systematically with increasing $x$ (cf. circles in Fig. 3(b)) as $E_{cutoff}^{high}(x)\,\text{eV} = (5.12\pm0.03)\,\text{eV} - (1.82\pm0.09)\,\text{eV}\cdot x$. On one hand, the high surface densities of photo-excited carriers cause a high surface recombination velocity resulting a reduced $\mathcal{R}$ for further increasing $\hbar\omega$. On the other hand, the systematic changing of $E_{cutoff}^{high}$ could be explained by an
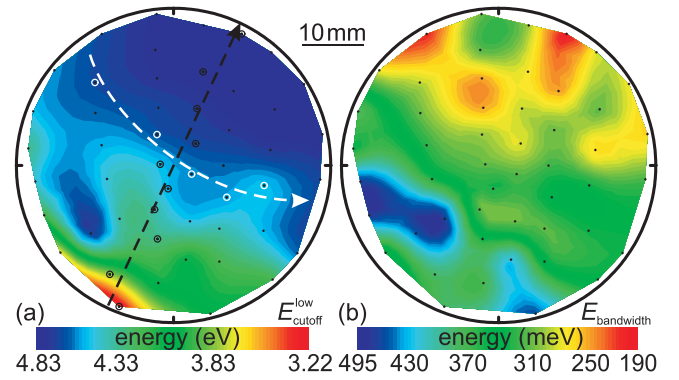
optical filter layer between the film and the substrate;[6,7] obviously, that is not the case for PDs investigated here. The appearance of a decreasing $E_{cutoff}^{high}$ for devices with increasing $x$ is now most likely due to an indiffusion of Al to $(In_xGa_{1-x})_2O_3$ alloy.[31] Compared to $(Mg,Zn)O$ alloy,[40] in which Al acts as a donor, the Al-diffusion from sapphire into the active layer results in an increased $E_g$ due to the formation of quaternary $(Al, In, Ga)_2O_3$ alloy.[41] This Al-interdiffusion has been observed in $\beta$-$Ga_2O_3$ during post-annealing.[42,43] The same behavior is observed in unintentionally doped sample by secondary neutral mass spectrometry (SNMS) to obtain the relative Al-incorporation along the growth direction. However, a similar effect of $E_{cutoff}^{high}$-shift was observed for PDs based on MgO substrate remained puzzling.[31] Fig. 3(c) shows the SNMS-depth profiles on two pieces from Ga- and In-rich region, for which the diffusion length was significant for both pieces showing enhanced Al-concentration with a thickness of about 170 and 250 nm highlighted by green dashed rectangles, respectively. Hence, the shift of $E_{cutoff}^{high}$ could be explained by such inhomogeneous "filter" layer. Note that the fall-off of $\mathcal{R}$ around $\hbar\omega = 5.0$ eV is attributed to the limitation of xenon arc lamp above 4.96 eV.

Fig. 3(d) shows increased film thickness from 580 to 845 nm with increasing $x$ determined by a Dektak XT mechanical profilometer. This can be explained by different growth rate of both ablated segments that along $[\bar{2}01]$ of monoclinic $\beta$-$Ga_2O_3$ is much lower than that of cubic bixbyite $In_2O_3$ along [111]. The width of the space charge region of related SCs based on binary $\beta$-$Ga_2O_3/In_2O_3$ can be determined of about 260/230 nm by $10^{17}$ cm$^{-3}$ at $-4.0$ V. Upon backside illumination, most of the incident irradiation is absorbed by $(In_xGa_{1-x})_2O_3$ film prior to reach the depletion region due to a small penetration depth of about 100 nm calculated from the absorption coefficient in Ref. 31. However, $\mathcal{R}$ of PDs, in particular, fabricated from In-rich part was sufficiently high. This could be caused by the phase separation depending on $x$, which results in an inhomogeneity of the In-profile along the growth orientation in the graded layer. To improve the device performance, further investigations are necessary.

A gain mechanism is observed (cf. Fig. 3(a)), however, only for PDs fabricated from the In-rich part. No gain mechanism was observed for PDs from the Ga-rich region, for which the reason remains unclear. $\mathcal{R}_{max.}$ of these four

TABLE I. Comparison of characteristic parameters of UV MSM-PDs.

| | $(In_xGa_{1-x})_2O_3$ | | | $Al_xGa_{1-x}N$ | $Mg_xZn_{1-x}O$ | $Ni_xMg_{1-x}O$ | $Zr_xTi_{1-x}O_2$ | Diamond |
|---|---|---|---|---|---|---|---|---|
| Ref. | This work | 27 | 34 | 2 | 5 | 8 | 9 | 11 |
| $x$ | 0.0035–0.83 | 0–0.2 | 0.153–0.184 | 0.07–0.4 | 0.5–0.7 | 0.52–1.0 | 0–0.3 | … |
| $E_{cutoff}^{low}$ (eV) | 4.83–3.22 | 4.77–4.43 | 4.59–4.0 | 3.7–4.63 | 4.32–5.51 | 4.2–4.07 | 3.9–4.9 | 5.64 |
| $\mathcal{R}_{max.}$ (mA/W) | 30–500 | 0.1–200 | 0.008–0.07 | 6–160 | 0.01 | … | $10^4$–$10^5$ | 6000 |
| SNR | $10$–$10^3$ | $10^2$–$10^4$ | $10^4$ | … | $10^4$ | … | $10^2$ | $10^8$ |
| $|V_{ext.}|$ (V) | 4 | 10 | 5 | 0.2–20 | 10 | 30 | 5 | 3 |

devices exceeds the theoretical maximum of external quantum efficiency $\eta = 1$ (cf. dashed-dotted line). To explain this effect, the spectrally resolved current-density voltage ($JV$) measurements of a SC from a sample piece with $x = 0.38$ under backside illumination were carried out and are depicted in Fig. 3(e). Upon 4.35 eV of $\mathcal{R}_{max.}$, the reverse $J$ increases by about one order at $-1.0$ V compared with that in dark condition. In the forward direction, with increasing $\hbar\omega$ the $\Phi_{Bn,eff}$ decreases and the ideality factor increases. By using the thermionic emission theory, $\Phi_{Bn,eff}$ has been determined from forward $J$ and depicted together with $\mathcal{R}$ in Fig. 3(a) as squares. A clear correlation between increasing $\mathcal{R}$ and decreasing $\Phi_{Bn,eff}$ is observed, indicating that the gain mechanism can be explained by trapping of photo-excited holes at metal/$(In_xGa_{1-x})_2O_3$ interface.[44,45]

Moreover, another effect was observed in Fig. 3(a) that $\mathcal{R}$ of each PD under the same $\hbar\omega$ increases with increasing $x$. Fig. 3(f) shows the dependence of increasing $\mathcal{R}_{max.}$ of PDs on $x$ (cf. open triangles). This can be attributed to the high forward $J$ of the corresponding SCs from In-rich part due to the higher conductivity and with that lower $R_S$. Solid triangles in Fig. 3(f) depict decreased $R_S$ for increasing $x$, which were determined from forward $J$ of the corresponding SCs.[32] Similar results were reported in Ref. 46 that as $x$ increased, the conductivity and carrier concentration increased.

Fig. 3(g) shows the $\mathcal{R}$-spectra of other 5 MSM-PDs, but for positions selected from a stripe with nearly the same $x$ along a line lying perpendicular to the In-gradient. The selected positions of PDs are indicated by white ring along white dashed arrow in Fig. 4(a). It makes fabrications of PDs with nearly the same absorption onset feasible. As can be seen in Fig. 3(h), both $E_{cutoff}^{low\,(high)}$ have only slight differences of $\Delta E_{cutoff}^{low\,(high)} = 115\,(60)$ meV for $\Delta x = 0.015$. These values are much smaller than the maximum difference of $\Delta E_{cutoff}^{low\,(high)} = 1.61\,(1.60)$ eV along the In-gradient.

The spatial dependence of $E_{cutoff}^{low}$ of all MSM-PDs is depicted in Fig. 4(a). $E_{cutoff}^{low}$ has the same spatial dependence as $x$ (cf. Fig. 2(a)). A red-shift of $E_{cutoff}^{low}$ is observed for increasing $x$, whereas they are essentially constant along lines lying perpendicular to the In-gradient. All $E_{cutoff}^{low}$ have been achieved from UVA to low energy part of UVC. Compared to PDs based on CCS (Mg, Zn)O thin films in wurtzite modification,[6,7] the results here expand the spectral range of irradiation detection from 3.22 to 4.83 eV. However, for SCs from In-rich part with a lower rectification ratio, it needs further optimization of the fabrication process. Due to existence of $E_{cutoff}^{high}$, the so-called "spectral bandwidth" $E_{bandwidth}$ defined as $E_{cutoff}^{high} - E_{cutoff}^{low}$ can be obtained and is shown in Fig. 4(b).

$E_{bandwidth}$ increases from 190 to 495 meV for increasing $x$, for which the $E_{cutoff}^{high}$ of PDs varies from 5.21 to 3.61 eV (cf. Fig. 3(b)). It is thus inspired that UV PDs with tunable narrow bandwidths can be enabled by deposition of an optical filter layer on the opposite side of the substrate. Besides, we list the characteristic parameters of our devices in Table I in comparison with other UV MSM-PDs reported in the literature.

In summary, we here demonstrate UV PDs based on a Si-doped $(In_xGa_{1-x})_2O_3$ thin film by the CCS-PLD approach relying on segmented target. The In-content ranged from 0.0035 to 0.83 with a variation of Si between 0.003 and 0.037. A crystallographic phase separation was observed from monoclinic $\beta$-$Ga_2O_3$ via hexagonal $InGaO_3$ (II) to cubic bixbyite $In_2O_3$. Backside illuminated MSM-PDs were characterized, for which the cutoff energy changed systematically from UVA to UVC spectral range from 3.22 to 4.83 eV. For PDs from In-rich part of $(In_xGa_{1-x})_2O_3$, due to higher conductivity, the higher photo response was observed and an internal gain mechanism was measured as well. The presented results imply that such UV PDs can be used for sensing applications within the whole visible-blind to partially solar-blind spectral range.

[1]M. Razeghi and A. Rogalski, J. Appl. Phys. **79**, 7433 (1996).
[2]M. Gökkavas, S. Butun, P. Caban, W. Strupinski, and E. Ozbay, Semicond. Sci. Technol. **27**, 065004 (2012).
[3]M. Brendel, M. Helbling, A. Knauer, S. Einfeldt, A. Knigge, and M. Weyers, Phys. Status Solidi A **212**, 1021 (2015).
[4]A. Ohtomo, M. Kawasaki, T. Koida, K. Masubuchi, H. Koinuma, Y. Sakurai, Y. Yoshida, T. Yasuda, and Y. Segawa, Appl. Phys. Lett. **72**, 2466 (1998).
[5]Z. G. Ju, C. X. Shan, D. Y. Jiang, J. Y. Zhang, B. Yao, D. X. Zhao, D. Z. Shen, and X. W. Fan, Appl. Phys. Lett. **93**, 173505 (2008).
[6]Z. Zhang, H. von Wenckstern, and M. Grundmann, Appl. Phys. Lett. **103**, 171111 (2013).
[7]Z. Zhang, H. von Wenckstern, and M. Grundmann, IEEE J. Sel. Top. Quantum Electron. **20**, 106 (2014).
[8]H. Nishitani, K. Ohta, M. Inada, T. Shimizu, S. Shingubara, and T. Saitoh, in *2015 IEEE International Meeting for Future of Electron Devices, Kansai (IMFEDK)* (2015), pp. 88–89.
[9]H. Zhang, C. Feng, C. Liu, T. Xie, J. Zhou, and S. Ruan, IEEE Electron Device Lett. **32**, 934 (2011).
[10]M. D. Whitfield, S. S. Chan, and R. B. Jackman, Appl. Phys. Lett. **68**, 290 (1996).

[11]M. Liao, L. Sang, T. Teraji, M. Imura, J. Alvarez, and Y. Koide, Jpn. J. Appl. Phys., Part 1 **51**, 090115 (2012).

[12]R. Bel Hadj Tahar, T. Ban, Y. Ohya, and Y. Takahashi, J. Appl. Phys. **83**, 2631 (1998).

[13]P. D. C. King, T. D. Veal, D. J. Payne, A. Bourlange, R. G. Egdell, and C. F. McConville, Phys. Rev. Lett. **101**, 116808 (2008).

[14]P. D. C. King, T. D. Veal, F. Fuchs, C. Y. Wang, D. J. Payne, A. Bourlange, H. Zhang, G. R. Bell, V. Cimalla, O. Ambacher, R. G. Egdell, F. Bechstedt, and C. F. McConville, Phys. Rev. B **79**, 205211 (2009).

[15]O. Bierwagen, J. S. Speck, T. Nagata, T. Chikyow, Y. Yamashita, H. Yoshikawa, and K. Kobayashi, Appl. Phys. Lett. **98**, 172101 (2011).

[16]C. Kranert, R. Schmidt-Grund, and M. Grundmann, Phys. Stat. Sol. RRL **8**, 554 (2014).

[17]H. von Wenckstern, D. Splith, F. Schmidt, M. Grundmann, O. Bierwagen, and J. S. Speck, APL Mater. **2**, 046104 (2014).

[18]I. Hamberg and C. G. Granqvist, J. Appl. Phys. **60**, R123 (1986).

[19]E. G. Víllora, K. Shimamura, Y. Yoshikawa, T. Ujiie, and K. Aoki, Appl. Phys. Lett. **92**, 202120 (2008).

[20]D. Splith, S. Müller, F. Schmidt, H. von Wenckstern, J. J. van Rensburg, W. E. Meyer, and M. Grundmann, Phys. Status Solidi A **211**, 40 (2014).

[21]S. Müller, H. von Wenckstern, D. Splith, F. Schmidt, and M. Grundmann, Phys. Status Solidi A **211**, 34 (2014).

[22]S. Müller, H. von Wenckstern, F. Schmidt, D. Splith, F.-L. Schein, H. Frenzel, and M. Grundmann, Appl. Phys. Express **8**, 121102 (2015).

[23]C. Sturm, J. Furthmüller, F. Bechstedt, R. Schmidt-Grund, and M. Grundmann, APL Mater. **3**, 106106 (2015).

[24]R. Hill, J. Phys. C **7**, 521 (1974).

[25]R. Shannon and C. Prewitt, J. Inorg. Nucl. Chem. **30**, 1389 (1968).

[26]F. Yang, J. Ma, C. Luan, and L. Kong, Appl. Surf. Sci. **255**, 4401 (2009).

[27]Y. Kokubun, T. Abe, and S. Nakagomi, Phys. Status Solidi A **207**, 1741 (2010).

[28]C. Kranert, J. Lenzner, M. Jenderka, M. Lorenz, H. von Wenckstern, R. Schmidt-Grund, and M. Grundmann, J. Appl. Phys. **116**, 013505 (2014).

[29]R. Schmidt-Grund, C. Kranert, T. Böntgen, H. von Wenckstern, H. Krauß, and M. Grundmann, J. Appl. Phys. **116**, 053510 (2014).

[30]F. Zhang, K. Saito, T. Tanaka, M. Nishio, and Q. Guo, Solid State Commun. **186**, 28 (2014).

[31]H. von Wenckstern, D. Splith, M. Purfürst, Z. Zhang, C. Kranert, S. Müller, M. Lorenz, and M. Grundmann, Semicond. Sci. Technol. **30**, 024005 (2015).

[32]H. von Wenckstern, D. Splith, A. Werner, S. Müller, M. Lorenz, and M. Grundmann, ACS Comb. Sci. **17**, 710 (2015).

[33]H. Peelaers, D. Steiauf, J. B. Varley, A. Janotti, and C. G. Van de Walle, Phys. Rev. B **92**, 085206 (2015).

[34]T.-H. Chang, S. Chang, W.-Y. Weng, C.-J. Chiu, and C.-Y. Wei, IEEE Photonics Technol. Lett. **27**, 2083 (2015).

[35]H. von Wenckstern, Z. Zhang, F. Schmidt, J. Lenzner, H. Hochmuth, and M. Grundmann, CrystEngComm **15**, 10020 (2013).

[36]R. Schewski, G. Wagner, M. Baldini, D. Gogova, Z. Galazka, T. Schulz, T. Remmele, T. Markurt, H. von Wenckstern, M. Grundmann, O. Bierwagen, P. Vogt, and M. Albrecht, Appl. Phys. Express **8**, 011101 (2015).

[37]*Pulsed Laser Deposition of Thin Films: Applications-Led Growth of Functional Materials*, edited by R. Eason (John Wiley & Sons, Inc., Hoboken, New Jersey, 2007).

[38]A. Lajn, H. v. Wenckstern, Z. Zhang, C. Czekalla, G. Biehne, J. Lenzner, H. Hochmuth, M. Lorenz, M. Grundmann, S. Wickert, C. Vogt, and R. Denecke, J. Vac. Sci. Technol. B **27**, 1769 (2009).

[39]M. Grundmann, *The Physics of Semiconductors, An Introduction including Nanophysics and Applications*, 3rd ed. (Springer-Verlag, Berlin, Heidelberg, 2016).

[40]H. von Wenckstern, R. Schmidt-Grund, C. Bundesmann, A. Müller, C. P. Dietrich, M. Stölzel, M. Lange, and M. Grundmann, "The (Mg,Zn)O alloy," in *Handbook of Zinc Oxide and Related Materials*, edited by Z. C. Feng (CRC Press, Boca Raton, FL, USA, 2012), Vol. 1, Chap. 10.

[41]C. Kranert, M. Jenderka, J. Lenzner, M. Lorenz, H. von Wenckstern, R. Schmidt-Grund, and M. Grundmann, J. Appl. Phys. **117**, 125703 (2015).

[42]M. Fleischer, W. Hanrieder, and H. Meixner, Thin Solid Films **190**, 93 (1990).

[43]G. Battiston, R. Gerbasi, M. Porchia, R. Bertoncello, and F. Caccavale, Thin Solid Films **279**, 115 (1996).

[44]O. Katz, G. Bahir, and J. Salzman, Appl. Phys. Lett. **84**, 4092 (2004).

[45]Z. Zhang, H. von Wenckstern, M. Schmidt, and M. Grundmann, Appl. Phys. Lett. **99**, 083502 (2011).

[46]L. Kong, J. Ma, F. Yang, C. Luan, and Z. Zhu, J. Alloys Compd. **499**, 75 (2010).